Advanced Air Mobility Electric Vertical Take-off Landing Aircraft Configuration and Concept Design Generation and Evaluation

Muhammad Fikri Zulkarnain, Taufiq Mulyanto, Hisar Manongam pasaribu & Ignatius Pulung Nurprasetio

Faculty of Mechanical and Aerospace Engineering, Institut Teknologi Bandung, Jl. Ganesa No.10, Bandung 40132, Indonesia
Email: zulkarnain.fikri@gmail.com

Abstract. In the modern day, Advanced Air Mobility, including electric vertical take-off landing (eVTOL) aircraft, is getting traction. However, not all possible configurations are modelled and compared to each other. A structured generation method is proposed in this study, by combining building blocks as well as parametric sizing. The proposed method in this paper can model multicopter, vectored thrust, independent thrust, and combined thrust configurations. Combined thrust is a configuration that has not been explored in other studies. The proposed method also allowed more combinations of alternatives by varying the number of rotors, which are fairly limited in other studies. Seventeen alternative configurations are generated and evaluated. The generated alternatives are evaluated by performing aerodynamic, power, energy, and weight analysis. The results of the analysis will be then compared to the requirements. The method proposed in this paper can analyze the differences between each configuration.

Keywords: *Advanced Air Mobility, Electric VTOL, Generation and Evaluation, Aircraft Configuration*

1 Introduction

Global warming, especially due to uncontrolled emissions, is a big challenge that can threaten the sustainability of human life in the future. Worldwide control efforts are currently ongoing, including in Indonesia. The government of Indonesia has planned a target for reducing greenhouse gas (GHG) emissions in Indonesia through Presidential Decree No. 18 of 2020 [1], as well as specifically in the field of air transportation in the Main Performance Indicators (IKU) of the Directorate General of Air Transportation for 2020-2024 [2]. In addition, several other problems related to transportation in Presidential Decree No. 18 of 2020 include the target of reducing potential losses due to congestion, as well as increasing access, especially for Frontier, Remote, and Disadvantaged Areas (3T Areas).

Advanced Air Mobility (AAM) is an air transportation system that moves people and cargo in areas that have not previously been or are still little served by using

Received ________, Revised _________, Accepted for publication __________

new and revolutionary technology [3]. The application of AAM can be in the form of transportation within the city in the form of Urban Air Mobility (UAM), as well as transportation of goods using unmanned vehicles (cargo drones) [4]. Preliminary studies have shown the potential benefits of AAM compared to current modes of transportation, including reduced levels of traffic congestion and lower emissions [4], [5]. While the IATA project air taxis operate in 2024 [6], most of AAMs are still under development [3].

NASA categorize AAM into three main configurations considered: wingless – such as multicopter, lift+cruise – two different power sources for vertical/hover flight and horizontal/forward flight; and vectored thrust – the same power source for vertical and horizontal flight [3]. Ugwueze [7] categorize the eVTOL aircraft into two main categories: wingless and powered flight. The powered flight includes vectored thrust, independent thrust, and combined thrust. The independent thrust is equivalent to lift+cruise configuration from NASA. However, the combined thrust is a hybrid configuration between lift+cruise and vectored thrust – there are power sources that can be used for vertical and horizontal flight and power sources only for vertical flight.

There are several studies related to the conceptual design of AAM. Balli [8] reverse engineers one helicopter and eleven AAM with multicopter, lift+cruise, and vectored thrust configuration, while Kadhiresan and Duffy [9] compares four configurations and one helicopter. While Ugwueze [7] initially discussing five AAM configurations which include the combined thrust configurations, the paper only elaborates on the vectored independent. Existing studies also limit the combination of configuration and number of rotors.

The aim and scope of this paper are to develop a structured descriptive modelling method which could model and generate eVTOL configurations. An analytical model. Develop an analytical model/method, which can compare the different configurations. The proposed method in this paper is designed to be able to model multicopter, vectored thrust, independent thrust, and combined thrust which has not been explored in other studies. The proposed method also allowed more combinations by varying the number of rotors, which are fairly limited in other studies.

2 Methodology

In this study, the methodology is divided into several parts, the generation method, and the evaluation method. The generation method will explain the structured generation model and how configuration can be constructed by building blocks. The generation of dimensions is also included in the generation method. Combinations of building blocks and dimensions will be called generated alternatives. The evaluation method will include aerodynamic, power, energy, and weight analysis of the generated alternatives.

For this paper, a simplified mission profile will be used as input for the generation. This mission profile includes three flight segments: (1) take-off, (2) cruise, and (3) land.

Each configuration is identified as a combination of building blocks, as shown in Figure 1. The main building blocks include: fuselage (all configurations have fuselage), wing+tail, vertical facing only rotor (V-rotor), horizontal/forward facing only rotor (H-rotor), and tilting rotor (V/H-rotor). For example, a multicopter (MC) configuration, only consists of fuselage and several V-rotor. A lift or cruise (L/C) configuration will have V/H-rotors for both lift generation during the hover flight and forward thrust during the cruise segment. There are two types of L/C configuration, an L/C Tilt-Wing (L/C TW) configuration (of which the whole wing or tail is tilted) or an L/C Tilt-Rotor (L/C TR) configuration (of which only the rotor-motor and part of nacelle will be tilted). A lift+cruise (L+C) and lift+lift or cruise (L+L/C) will have V-rotor building blocks, which will provide lift during the hover flight segment, but stop during the cruising flight segment (stopped rotor). An H-rotor will provide forward thrust during the cruise flight segment for L+C configurations, while V/H-rotors will provide both vertical lift during the hover flight segment and forward thrust during the cruise flight segment. An identifier for the tilt-wing is added to differentiate L/C TR and L/C TW configuration. MC configurations have motor arms, while other configurations have motor nacelle. Landing gears (LG) are added as an additional building block that every configuration has. The building blocks for 5 configurations are shown in Table 1.

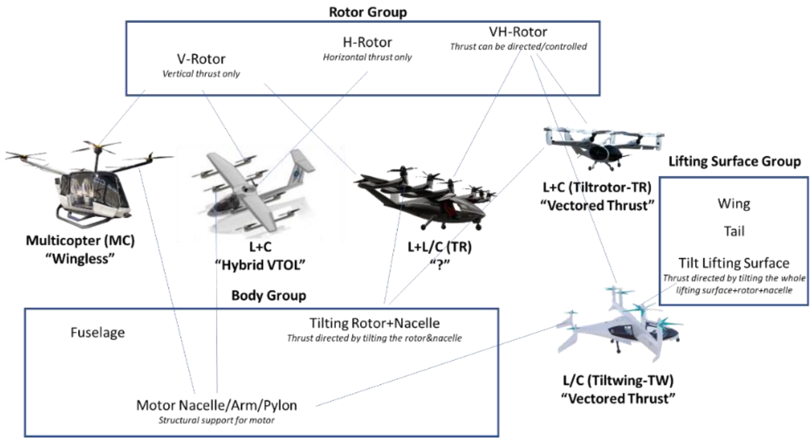

Figure 1 Building Blocks of eVTOL Aircraft.

Table 1 Building Blocks for 5 Configurations

	Fuselage	**Wing+Tail**	**TiltWing?**	**V;V/H;H Rotor**	**LG**
MC	Yes	No	No	V-rotor	Yes
L/C TW	Yes	Yes	Yes	V/H-rotor	Yes
L/C TR	Yes	Yes	No	V/H-rotor	Yes
L+C	Yes	Yes	No	V and H-rotor	Yes
L+L/C	Yes	Yes	No	V and V/H-rotor	Yes

Table 2 Dimension Generation Table

Building Blocks	**Value Parameter**	**Symbol**	**Dimension**	**Value**
Wing	Area	S_w	m^2	15
	Aspect Ratio	AR_w	-	10
	Chord	C_w	m	1.22
Fuselage	Length	L_f	m	5.3
	Diameter	D_f	m	1.3
	Wetted Area	$Swet_f$	m^2	33
Tail	Area		m^2	3.8
	Aspect Ratio		-	4.7
Rotor	Total Disk Area	S_d	m^2	28.3
	Number of Rotor	N_r	-	Variable
	Area per rotor	S_r	m^2	S_d/N_r
	Rotor Diameter	D_r	m	$\boldsymbol{2\sqrt{S_r/\pi}}$
	Chord at 75%	C_r	m	$0.1D_r$
Motor Arm	Length	L_a	m	$0.6D_r \sin(\pi/N_r)$
	Width	W_a	m	$0.1D_r$
Motor Nacelle	Length	Ln	m	$D_r/2 + C_w/2$
	Width	Wn	m	$0.1D_r$

For this study, the fuselage, wing, and tail dimensions, as well as total disk area are assumed to be the same for every configuration. The other dimensions are parametric, such as shown in Table 1. The motor arm, motor support, and motor nacelle dimensions are in proportion to the rotor dimensions. Typical arm/support/nacelle proportions are obtained from studying the geometry and proportions of existing aircraft. The width of the motor arm or nacelle is assumed to be 10% of the diameter of the rotor. The length of the nacelle is assumed to be the radius of the propeller plus half of the wing chord. The length of the motor arm must be such that same angle between adjacent arms, and no interference between each rotor. By building several geometry models on openVSP, an equation is developed as shown in Table 2.

An analytic method for aerodynamic analysis is used in this paper. The aerodynamic analysis will be used to estimate the drag coefficient. The method used in this paper is drag breakdown, which estimates the drag coefficient by calculating the friction components of the drag, and then multiplies the friction components with the pressure drag components (Form Factor-FF) and interference drag components (Q).

$$\Delta CD_c = \frac{C_{f_c} FF_C Q_C S_{wet}}{S_{ref}} \tag{1}$$

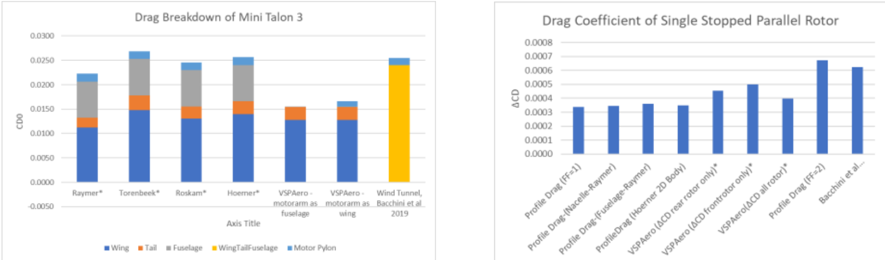

(a) (b)

Figure 2 Comparing several methods for: (a) wing, tail, fuselage, and motor pylon, and (b) stopped rotor.

Table 3 Chosen Method for Aerodynamic Analysis

Building Blocks	Q	FF
Wing	1	Hoerner
Tail	1.03	Hoerner
Fuselage	1	Raymer - Fuselage
Motor Nacelle	1.5	Raymer - Nacelle
Motor Arm	1.5	Raymer-Nacelle
Stopped Rotor – Parallel	Q*FF = 2	

There are already methods to estimate the FF and Q for fuselage, wing, tail, and nacelle in references such as Raymer [10], Torenbeek[11], Roskam[12], and Hoerner.[13] Method for motor arm and stopped rotor are not found. An OpenVSP [14] aerodynamic model can also be used to obtain drag. Thus, a case study is performed to compare the different methods, using geometry and then compared to the wind tunnel results from reference [15]. The comparison result is shown in Figure 2. From this, the methods chosen are Hoerner for Wing and Tail, Raymer for Fuselage and Nacelle, and Q*FF=2 for stopped rotor. The resume is shown in Table 3.

The power required during each flight segment can be categorized into three. The power required during hover, climb, and cruise by using vertical thrust provided by any combination of V-rotor and V/H-rotor. The power required during the climb and cruise segment using forward thrust is provided by any combination of V/H-rotor and H-rotor. And transition segment which may combine two methods.

The power required during hover can be estimated by equation (2) [16]. The power required divided by total disk area, is a function of the Figure of Merit (M), air density, and the disk loading (aircraft weight divided by total disk area). The Figure of Merit (M) is calculated using equation (3). The $C_T^{1.5}/\sqrt{2}$ component represents the ideal power required due to induced power, the $\sigma\delta/8$ component represents the power required due to profile drag, while κ represents the factor for the maximum attainable Figure of Merit. The typical value $\sigma\delta/8$ is assumed 0.00025. The value of κ is 1.15 for the general rotor and 1.334 for the coaxial rotor.

$$\left(\frac{P_{hover}}{S_{disk}}\right) = \sqrt{2\rho}\ \frac{M}{\sqrt{\frac{W_{aircraft}}{S_{disk}}}} \tag{2}$$

$$M = \frac{\frac{C_T^{1.5}}{\sqrt{2}}}{\kappa\frac{C_T^{1.5}}{\sqrt{2}} + \frac{\sigma\delta}{8}} \tag{3}$$

The coefficient of thrust (C_T) is a function of aircraft weight, total disk area (S), air density (ρ), and tip speed (ωR) as shown in equation (4). The induced velocity (v_h) is a function of tip speed (ωR) and coefficient of thrust (C_T) as shown in equation (5). This can be rearranged as a function of aircraft weight, total disk area (S), and air density (ρ). Thus, we could rearrange the coefficient of thrust (CT) as only a function of induced velocity (v_h) and tip speed (ωR) as in equation (6). The tip speed is assumed to be 180 m/s.

$$C_T = \frac{W_{aircraft}}{S_{disk}\rho(\omega R)^2} \tag{4}$$

$$v_h = \omega R\sqrt{\frac{C_T}{2}} = \sqrt{\frac{W_{aircraft}}{2\rho S_{disk}}} \tag{5}$$

$$C_T = 2\left(\frac{v_h}{\omega R}\right)^2 \tag{6}$$

The power required during hover must also account for two other factors: download and one engine inoperative. Download due to induced velocity enacted to the aircraft body below the rotor which resulted in downward force. Thus, extra power is needed to counteract this download (%d). The second factor is one engine-off requirement. During one engine-off case, the remaining motor, minus one motor for balancing purposes, must still be able to provide the required power. When in one engine inoperative (OEI) condition, the aircraft must have the ability to provide adequate lift during hover. For multicopter, to counterbalance torque, typically one other engine is also shut down. The OEI factor (k_{oei}) is equal to $n_r/(n_r-2)$ if the number of rotors is more than 4, and equal to 1.5 for other cases.

$$P_h = P_h(1 + \%d)k_{OEI} \qquad (7)$$

There is no established method to estimate download during conceptual design However, by plotting download and the projected download area (projected area under a rotor disk) from several references [17], [18], [19], [20] as shown in Figure 3, a pattern can be discerned. The higher the projected download area (%da), the higher the download (%d). Three lines representing the ratio of %download and %downloadarea are also shown in the figure. The aerodynamic model using OpenVSP also shows the pattern. Thus, for this study, the download is estimated to be equal to the download area (%d/%da) for general geometry, and equal to 75% download area for flapped wing.

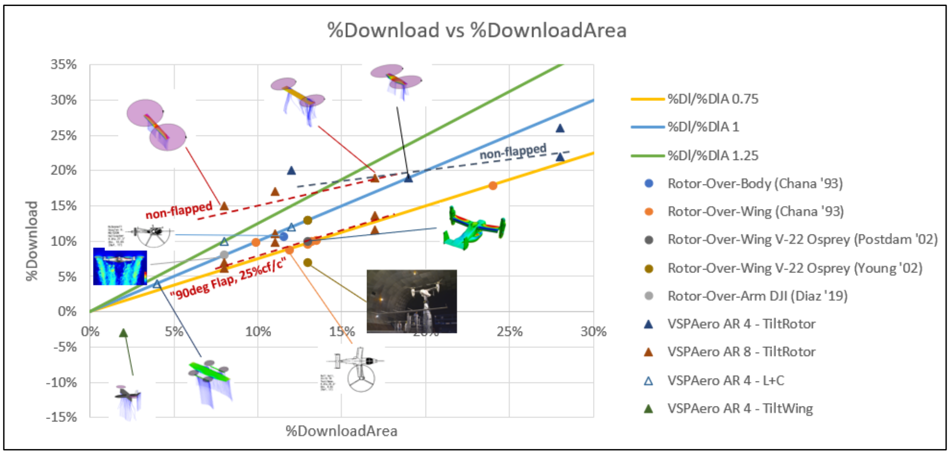

Figure 3 Correlation between download and download area.

At the climb flight segment using vertical thrust only, the climb power (P_{cl}) can be calculated using equation (8). The ratio between climb power and hover power is a function of the Rate of Climb (Roc) and induced velocity.

$$\frac{P_{cl}}{P_{hv}} = \frac{RoC}{2v_h} + \sqrt{\left(\frac{RoC}{2v_h}\right)^2 + 1} \qquad (8)$$

Cruise flight segment using V-rotors can be calculated using equation (9), which consists of the power required to counter the profile drag of the rotor (L/D_0), induced drag due to lift generation (L/D_i), and profile drag of the aircraft (L/D_p) [21]. Equation (10), (11), and (12) is used to estimate (L/D_0), (L/D_i), (L/D_p).

$$\frac{W_{aircraft}}{P_{cruise}} = \left(\left(\frac{L}{D}\right)_0\right)^{-1} V + \left(\left(\frac{L}{D}\right)_i\right)^{-1} V + \left(\left(\frac{L}{D}\right)_p\right)^{-1} V \tag{9}$$

$$\left(\left(\frac{L}{D}\right)_0\right)^{-1} = \frac{\sigma\delta(1 + 3\mu^2 + 0.375\mu^4)}{8\mu C_T} \tag{10}$$

$$\left(\left(\frac{L}{D}\right)_i\right)^{-1} = D.L.\frac{1}{4q} \tag{11}$$

$$\left(\left(\frac{L}{D}\right)_p\right)^{-1} = \frac{qS_{disk}C_{D_p}}{W_{aircraft}} \tag{12}$$

During climb and cruise flight segments using horizontal thrust only, the power required can be calculated using equation (13) [22] accounting the required power for cruising, and for forward-climbing, denoted by RoC). The power required that needs to be supplied to the electric motor, accounting for the propeller efficiency, then can be calculated using equation (14).

$$P_{req} = W * \left(\left(\frac{L}{D}\right)^{-1} V + RoC\right) \tag{13}$$

$$P_{shaft_h} = \frac{P_{req}}{\eta_p} \tag{14}$$

The total energy required is the sum of energy required at each flight segment, as shown in equation (15). The energy required at each flight segment is the product of power during each flight segment and the duration of each flight segment. However, the total energy provided by the battery must account for the minimum State of Charge (SoC). The typical SoC is assumed to be 20%.

$$E_{req} = \sum P_{flightsegment} t_{flightsegment} \tag{15}$$

$$E_{req,soc} = \frac{E_{req}}{(1 - SoC)} \tag{16}$$

The total weight of the aircraft is the sum of payload, battery, airframe, propulsion, and fixed equipment as shown in equation (17). For the airframe and system, Nicolai/Balli method [8] is used. An extra factor from NASA/NDARC [23] will be used, as the Nicolai/Balli method does not account for tilt-wing configuration. The battery density battery was initially assumed to be 250 Wh/kg [24].

$$m_{to} = m_{payload} + m_{batt} + m_{airframe} + m_{propulsion} + m_{fixed,eq.} \tag{17}$$

For this paper, the maximum takeoff weight is set as a constraint, with a value of 3200 kg. The battery weight is obtained by subtracting the MTOW from the airframe, system, propulsion, payload, and operating weight. The battery energy for cruise flight is then calculated by subtracting the total battery energy from the energy required for hover, transition, and SoC.

3 Results and Discussion

Figure 4 illustrates 17 generated alternative combinations of configuration and number of V-rotors generated. Generated alternatives correspond to existing eVTOL configurations. For example, there are no L/C configurations with more than 8 V/H rotors, and there are no L+C and L+L/C configurations with more than 12 V-rotors. The red area represents combinations that have no real-world examples, or in the case of 2 V-rotors MC, is a helicopter which is outside the scope of this paper. While the orange area represents combinations that real-world examples such as small AAM (drones).

MC configurations have the least drag due to not having a wing and tail, as shown in Figure 5. However, MC also has the lowest Lift-to-Drag ratio. This may be due to due induced drag of the rotor being higher compared to the wing. The higher number of rotors also corresponds to the increase in pylon drag. Drag due to the stopped rotor of L+L/C and L+C adds significant drag. L/C configurations have the highest Lift-to-Drag ratio.

A comparison of power calculation is shown in Figure 6. The configuration with the least hover power is L/C TW with 8 rotors. This is due to the tilt-wing configuration having no download, and 8 rotors requiring less OEI. Meanwhile, L/C TR with 2 and 4 rotors requires the highest hover power due to the higher download and OEI factor.

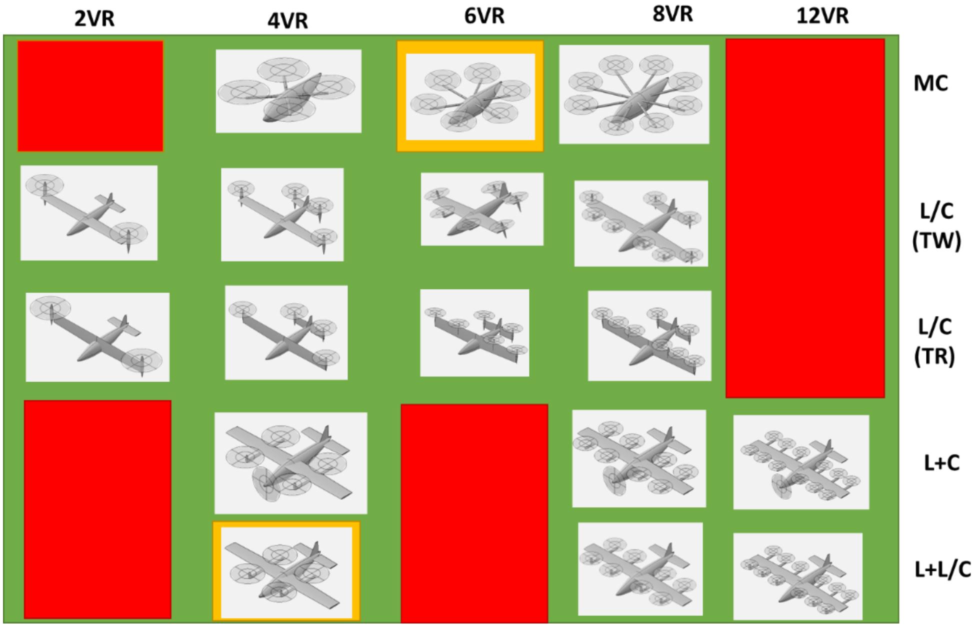

Figure 4 Generated eVTOL configuration alternatives.

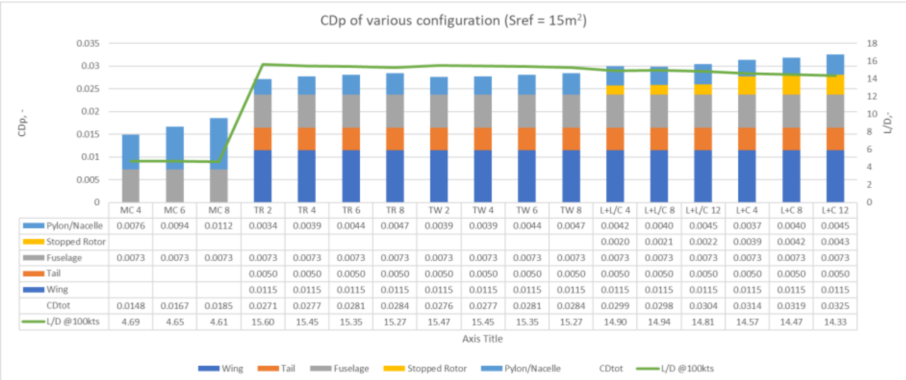

	MC 4	MC 6	MC 8	TR 2	TR 4	TR 6	TR 8	TW 2	TW 4	TW 6	TW 8	L+L/C 4	L+L/C 8	L+L/C 12	L+C 4	L+C 8	L+C 12
Pylon/Nacelle	0.0076	0.0094	0.0112	0.0034	0.0039	0.0044	0.0047	0.0039	0.0039	0.0044	0.0047	0.0042	0.0040	0.0045	0.0037	0.0040	0.0045
Stopped Rotor												0.0020	0.0021	0.0022	0.0039	0.0042	0.0043
Fuselage	0.0073	0.0073	0.0073	0.0073	0.0073	0.0073	0.0073	0.0073	0.0073	0.0073	0.0073	0.0073	0.0073	0.0073	0.0073	0.0073	0.0073
Tail				0.0050	0.0050	0.0050	0.0050	0.0050	0.0050	0.0050	0.0050	0.0050	0.0050	0.0050	0.0050	0.0050	0.0050
Wing				0.0115	0.0115	0.0115	0.0115	0.0115	0.0115	0.0115	0.0115	0.0115	0.0115	0.0115	0.0115	0.0115	0.0115
CDtot	0.0148	0.0167	0.0185	0.0271	0.0277	0.0281	0.0284	0.0276	0.0277	0.0281	0.0284	0.0299	0.0298	0.0304	0.0314	0.0319	0.0325
L/D @100kts	4.69	4.65	4.61	15.60	15.45	15.35	15.27	15.47	15.45	15.35	15.27	14.90	14.94	14.81	14.57	14.47	14.33

Figure 5 Drag coefficient breakdown and L/D ratio for each alternative.

MC configurations have the highest cruise power, due to MC having the lowest lift-to-drag ratio. However, L/C with 2 rotors have the least cruise power required, due to having the highest lift-to-drag ratio. Thus, while a higher number of rotors provides lower hover power due to a reduction in OEI factor, a lower number of rotors provides lower cruise power due to the reduction of drag provided by pylons.

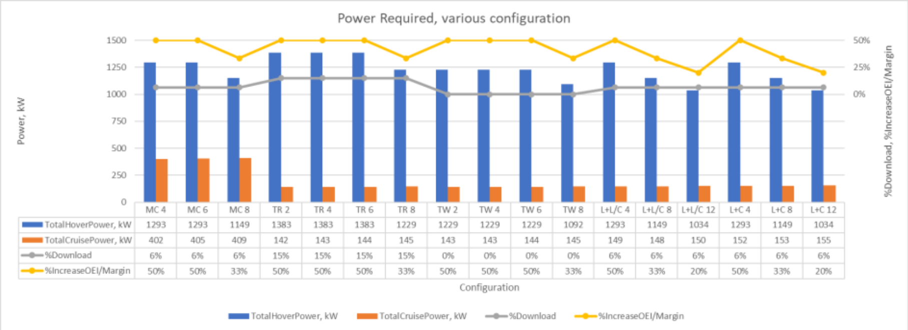

	MC 4	MC 6	MC 8	TR 2	TR 4	TR 6	TR 8	TW 2	TW 4	TW 6	TW 8	L+L/C 4	L+L/C 8	L+L/C 12	L+C 4	L+C 8	L+C 12
TotalHoverPower, kW	1293	1293	1149	1383	1383	1383	1229	1229	1229	1229	1092	1293	1149	1034	1293	1149	1034
TotalCruisePower, kW	402	405	409	142	143	144	145	143	143	144	145	149	148	150	152	153	155
%Download	6%	6%	6%	15%	15%	15%	15%	0%	0%	0%	0%	6%	6%	6%	6%	6%	6%
%IncreaseOEI/Margin	50%	50%	33%	50%	50%	50%	33%	50%	50%	50%	33%	50%	33%	20%	50%	33%	20%

Figure 6 Power breakdown for each alternative.

MC configuration has the least airframe weight compared to other configurations due to not having a wing. The other configurations have very similar airframe weight. The propulsion weight directly correlates with the power requirements, thus configurations with a higher number of motors typically have lower propulsion weight. The L/C and L+L/C configurations have higher fixed equipment weight, as they need to allocate weight for the tilting (L/C) mechanism. L/C Tilt-wing configurations have the highest fixed equipment weight due to the need to tilt the entire wing.

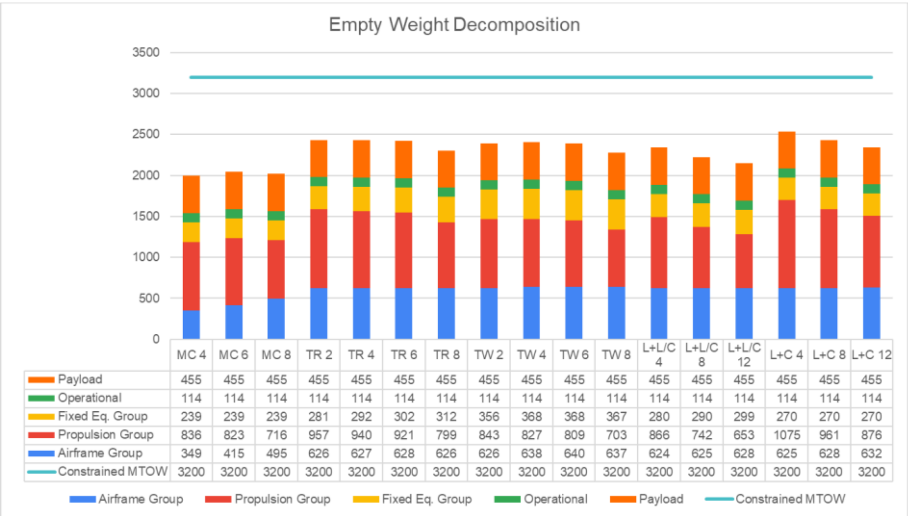

	MC 4	MC 6	MC 8	TR 2	TR 4	TR 6	TR 8	TW 2	TW 4	TW 6	TW 8	L+L/C 4	L+L/C 8	L+L/C 12	L+C 4	L+C 8	L+C 12
Payload	455	455	455	455	455	455	455	455	455	455	455	455	455	455	455	455	455
Operational	114	114	114	114	114	114	114	114	114	114	114	114	114	114	114	114	114
Fixed Eq. Group	239	239	239	281	292	302	312	356	368	368	367	280	290	299	270	270	270
Propulsion Group	836	823	716	957	940	921	799	843	827	809	703	866	742	653	1075	961	876
Airframe Group	349	415	495	626	627	628	626	626	638	640	637	624	625	628	625	628	632
Constrained MTOW	3200	3200	3200	3200	3200	3200	3200	3200	3200	3200	3200	3200	3200	3200	3200	3200	3200

Figure 7 Weight decomposition for each alternative.

Out of 17 configurations, only L+L/C with 12 rotors have a range of at least 100 nm, as shown in Figure 8. The second configuration is L+L/C with 8 rotors (94 nm) and the third configuration is L/C tilting with 8 rotors (90 nm). This is mainly due to the relatively higher battery weight and relatively lower cruise and hover power. MC configurations, while having the highest battery weight, have the lowest range. This is due to the MC configuration having the highest cruise power. The range can be increased by possible future technologies such as weight reduction due to advanced composites airframe and higher battery density.

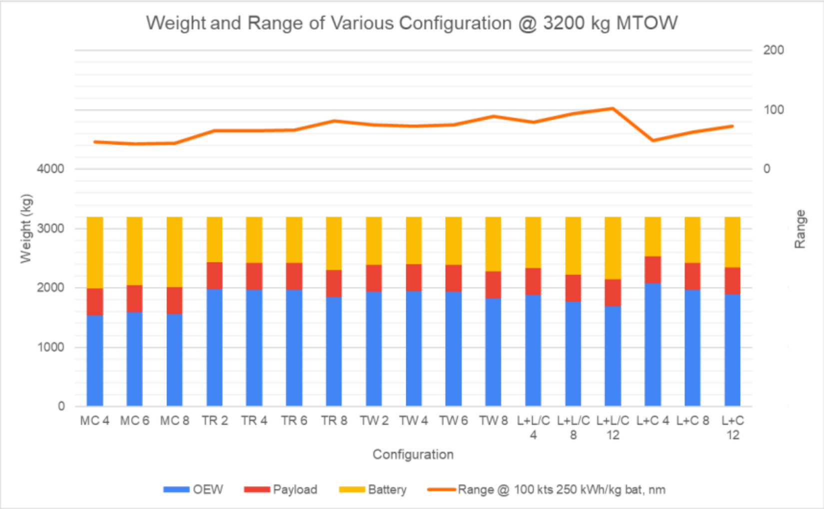

Figure 8 Range comparison of generated alternatives.

4 Conclusion

A method to structurally generate AAM eVTOL alternative configuration has been done in this paper. The generation includes combining building blocks to create a configuration, as well as parametric generation of dimensions. The building blocks can be combined to make five main configurations: Multicopter, L/C Tilt-Wing, L/C Tilt-Rotor, L+C, and L+L/C. Extra configurations are made by varying the number of V-rotors. Seventeen configurations have been generated and evaluated in this paper. The evaluation of alternative configurations consists of aerodynamic, power, energy, and weight analysis. The method proposed in this paper can analyze the differences between each configuration.

For future research, other use case studies will need to be performed in the future too. The structured generation can also be improved to generate more alternatives by varying other parameters such as MTOW, wing area, or disk area. Better integration and automation between the structured generation model and the analytical model are needed to deal with the increase in computation demand for more alternatives. Implementation of Model-based Systems Engineering Framework such as performed by Specking et al [25], can be a solution for the integration and automation of structured and analytic models.

5 References

[1] Pemerintah RI, ‘PERPRES No. 18 Tahun 2020 tentang Rencana Pembangunan Jangka Menengah Nasional Tahun 2020-2024 [JDIH BPK RI]’. Accessed: Mar. 15, 2023. [Online]. Available: https://peraturan.bpk.go.id/Home/Details/131386/perpres-no-18-tahun-2020

[2] Direktorat Jenderal Perhubungan Udara RI, ‘Buku Profil Direktorat Jenderal Perhubungan Udara Edisi September 2022’. 2022. [Online]. Available: https://hubud.dephub.go.id/hubud/website/IPBukuProfil.php

[3] NASA, ‘Advanced Air Mobility Mission Overview’, NASA. Accessed: Jan. 07, 2023. [Online]. Available: http://www.nasa.gov/aam/overview

[4] EASA, ‘Study on the societal acceptance of Urban Air Mobility in Europe’. 2021. [Online]. Available: https://www.easa.europa.eu/sites/default/files/dfu/uam-full-report.pdf

[5] J. Michelmann, A. Straubinger, A. Becker, C. A. Haddad, K. O. Plötner, and M. Hornung, ‘URBAN AIR MOBILITY 2030+: PATHWAYS FOR UAM – A SCENARIO- BASED ANALYSIS’, presented at the Deutscher Luft- und Raumfahrtkongress 2020, 2020.

[6] IATA, ‘Aircraft Technology Roadmap to 2050’, 2019.

[7] O. Ugwueze, T. Statheros, N. Horri, M. A. Bromfield, and J. Simo, ‘An Efficient and Robust Sizing Method for eVTOL Aircraft Configurations in Conceptual Design’, *Aerospace*, vol. 10, no. 3, Art. no. 3, Mar. 2023, doi: 10.3390/aerospace10030311.

[8] M. E. Balli, ‘eVTOL AIRCRAFT CONCEPTUAL DESIGN AND OPTIMIZATION’, Master Thesis, 2020.

[9] A. R. Kadhiresan and M. J. Duffy, ‘Conceptual Design and Mission Analysis for eVTOL Urban Air Mobility Flight Vehicle Configurations’, in *AIAA Aviation 2019 Forum*, in AIAA AVIATION Forum. , American Institute of Aeronautics and Astronautics, 2019. doi: 10.2514/6.2019-2873.

[10] D. P. Raymer, *Aircraft Design: A Conceptual Approach*, 2nd ed. Washington, D.C.: AIAA, 1992.

[11] E. Torenbeek, *Synthesis of Subsonic Airplane Design*. Dordrecht: Springer Netherlands, 1982. doi: 10.1007/978-94-017-3202-4.

[12] J. Roskam, *Airplane Design Part VI: Preliminary Calculation of Aerodynamic, Thrust and Power Characteristics*. 1985. Accessed: Nov. 29, 2024. [Online]. Available: https://shop.darcorp.com/index.php?route=product/product&product_id=59

[13] Sighard F. Hoerner, *Fluid-Dynamic Drag*. 1965. Accessed: Nov. 29, 2024. [Online]. Available: http://archive.org/details/FluidDynamicDragHoerner1965

[14] ‘OpenVSP’. Accessed: Nov. 29, 2024. [Online]. Available: https://openvsp.org/
[15] A. Bacchini, E. Cestino, B. Van Magill, and D. Verstraete, ‘Impact of lift propeller drag on the performance of eVTOL lift+cruise aircraft’, *Aerospace Science and Technology*, vol. 109, p. 106429, Feb. 2021, doi: 10.1016/j.ast.2020.106429.
[16] J. G. Leishman, *Principles of Helicopter Aerodynamic*. Cambridge University Press, 2006.
[17] W. Chana and T. Sullivan, ‘Download - The tilt rotor’s downfall’, in *International Powered Lift Conference*, American Institute of Aeronautics and Astronautics, 1993. doi: 10.2514/6.1993-4814.
[18] L. Young, D. Lillie, M. McCluer, G. Yamauchi, and M. Derby, ‘Insights into Airframe Aerodynamics and Rotor-on-Wing Interactions from a 0.25-Scale Tiltrotor Wind Tunnel Model’, Jan. 2002.
[19] M. A. Potsdam and R. C. Strawn, ‘CFD Simulations of Tiltrotor Configurations in Hover’, *Journal of the American Helicopter Society*, vol. 50, no. 1, pp. 82–94, Jan. 2005, doi: 10.4050/1.3092845.
[20] P. Diaz and S. Yoon, ‘Computational Analysis of Urban Air Mobility Vehicles’, 2019. Accessed: Nov. 29, 2024. [Online]. Available: https://www.semanticscholar.org/paper/Computational-Analysis-of-Urban-Air-Mobility-Diaz-Yoon/cda265d07534472593df04a8d0eb41a5e38208f8
[21] A. Gessow and G. C. Myers Jr., *Aerodynamics of the Helicopter*. Frederick Ungar Publishing Co., 1985.
[22] G. J. J. Ruijgrok, *Elements of airplane performance*. VSSD, 2009.
[23] J. Wayne, ‘NASA Design and Analysis of Rotorcraft’, NASA/TP-2015-218571, 2015.
[24] X. Qiao, G. Chen, W. Lin, and J. Zhou, ‘The Impact of Battery Performance on Urban Air Mobility Operations’, *Aerospace*, vol. 10, no. 7, Art. no. 7, Jul. 2023, doi: 10.3390/aerospace10070631.
[25] E. Specking, G. Parnell, E. Pohl, and R. Buchanan, ‘Early Design Space Exploration with Model-Based System Engineering and Set-Based Design’, *Systems*, vol. 6, no. 4, Art. no. 4, Dec. 2018, doi: 10.3390/systems6040045.